Future Computing and Informatics Journal

Volume 3
Issue 2 *Vol 3,Issue 2,2018*

Article 11

2018

Feature based transition region extraction for image segmentation: Application to worm separation from leaves

Priyadarsan Parida
GIET University, priyadarsan.vssut@gmail.com

Nilamani Bhoi
Department of Electronics & Telecommunication Engineering, Veer Surendra Sai University of Technology, Burla 768018, Sambalpur, India, nilamanib@gmail.com

Available online at www.sciencedirect.com

ScienceDirect

Future Computing and Informatics Journal 3 (2018) 262–274
http://www.journals.elsevier.com/future-computing-and-informatics-journal/

Feature based transition region extraction for image segmentation: Application to worm separation from leaves

Priyadarsan Parida [a,*], Nilamani Bhoi [b]

[a] Department of Electronics and Communication Engineering, Gandhi Institute of Engineering & Technology, Gunupur, Rayagada, 765022, Odisha, India
[b] Department of Electronics and Telecommunication Engineering, Veer Surendra Sai University of Technology, Burla, Sambalpur, 768018, Odisha, India

Received 26 October 2017; revised 20 March 2018; accepted 1 August 2018
Available online 9 August 2018

Abstract

Transition region based approaches are recent hybrid segmentation techniques well known for its simplicity and effectiveness. Here, the segmentation effectiveness depends on robust extraction of transition regions. So, we have proposed transition region extraction method for image segmentation. The proposed method initially decomposes the gray image in wavelet domain. Local standard deviation filtering and thresholding operation is used to extract transition region feature matrix. Using this feature matrix, the corresponding prominent wavelet coefficients of different bands are found. The inverse wavelet transform is then applied to the modified coefficients to get edge image with more than one-pixel width. Global thresholding is applied to get transition regions. Further, it undergoes morphological thinning and region filling operation to extract the object regions. Finally, the objects are extracted using the object regions. The proposed method is compared with different image segmentation methods. An experimental result reveals that the proposed method outperforms other methods for segmentation of images containing single and multiple objects. The proposed method can also be applied for worm separation from leaves.

Keywords: Transition region; Otsu thresholding; Features; Morphological operation

1. Introduction

Image segmentation is an important pre-processing step for all computer vision and image understanding tasks. It has a wide range of applications such as biometrics [1], medical image analysis [2], crop disease detection and classification [3], etc. Image segmentation is the process of separating the object (foreground) from background considering certain features of the image such as colour, intensity, texture, etc. In the past decade, a wide variety of segmentation techniques are available in literature. In the recent era several hybrid segmentation techniques have been emerged which provide better segmentation results compared to that of the traditional methods. These hybrid segmentations are classified as model based segmentation approaches [4,5], machine learning approaches [6], graph-cut methods [7], active contour and level set methods [8–11] and transition region based approaches [12–21]. In the model based approaches, the image is characterised by a statistical model and the model parameters are used as features for segmentation [22]. The machine learning process is basically a training process where a network is trained to optimize the weights of the network from training images features like texture, brightness, etc. After training, the network is presented the query image, and it performs classification based segmentation from the tuned weights and learned weights [6]. Graph cut based approaches consider the image as a weighted graph with nodes and vertices where nodes represent pixels or voxels and vertices represent neighbourhood relationship between pixels. A cost function which represents the

* Corresponding author.
E-mail addresses: priyadarsan.vssut@gmail.com (P. Parida), nilamanib@gmail.com (N. Bhoi).
Peer review under responsibility of Faculty of Computers and Information Technology, Future University in Egypt.

https://doi.org/10.1016/j.fcij.2018.08.001

cut is optimal in the sense that it effectively separates the object from the background [7]. Active contour based approaches deform its shape in the presence of external and internal forces leading the contour towards object [9]. In edge-based active contour methods image gradient is used to detect object boundaries [10] whereas region-based active contours use the object and background regions to find an energy optimum where the model fits the image to its best [11]. Level set methods usually make use of an edge indicator to pull the zero level set toward the desired object boundaries [9]. Transition region based methods [12–20] uses transition region for segmentation of images.

2. Related work

The transition region based approach is a hybrid approach which uses region-based segmentation and thresholding for locating the effective transition regions in an image. In an image the existence of transition region was initially demonstrated by Gerbrands et al. [12]. The transition regions are basically a 2-D regions whose gray level intensity lies between the gray level intensities of the objects and background. They further claimed that transition regions always exist for any image containing object and background. So, many researchers have proposed different approaches for appropriate extraction of transition region in an image, which in turn leads to achieve better segmentation results. In local entropy (LE) based method [19] the entropy of a neighborhood is considered to determine the transition region. It has a limitation that in the event of frequent changes in gray level in a local area; it increases the local entropy and the pixels in the neighborhood is identified as the transition region and it belongs to the foreground or the background. To overcome these disadvantages, Li et al. [17] developed a method for local extraction of the transition region based on the gray level difference (LGLD) which takes into account both changes in gray levels and the extent of these changes. However, the parameter selection unit for determining the threshold value is a problem. The modified local entropy method (MLE) [14] was then put in place to improve the extraction of the transition region. This method also suffers from the same problem as in LGLD. These techniques are ineffective when the foreground and background are of varying intensities. These are mainly used for images that contain a single object. A recent transition region based method named robust single-object image segmentation (RIB) proposed by Zuoyong Li et al. [13] is based on salient transition region provides good segmentation results. But, it only applies to images that contain a single object. To mitigate the limitation, Parida et al. [15] proposed local variance and morphological operator based method to yield better performance for both single and multiple object segmentation. In this method the images are categorized into four classes based on whether the background and foreground are simple or textured. The performance of the method degrades when the method is applied on images with (i) textured background and (ii) overlapping gray levels between foreground and background. To improve the performance, Parida et al. [18] proposed a novel method using 2-D Gabor filter for transition region. This method works well for overlapping gray levels between background and foreground.

3. Motivation

The method proposed by Parida et al. [18] is unable to perform well when the image contains textured background. Also, it has been found that the proposed method [18] cannot outperform Parida et al. [15] when both the background and foreground are simple. The transition regions of two different methods which work well for images containing single and multiple objects along with the proposed method are shown in Fig. 1 for Boat image taken from Wisemann dataset [23]. The segmentation results of the corresponding methods are shown in Fig. 2. The Fig. 1(a) shows the original Boat image and the red encircled region is zoomed and shown in Fig. 1(b). Fig. 1(c) shows the transition region of Parida et al. [15] and the corresponding zoomed region R is shown in Fig. 1(f) where the double headed blue lines show the point of discontinuity. It can be seen from the enlarged region of R that there exist some discontinuity marked in two blue lines in the regions which results in distorted segmentation mask affecting the overall segmentation result. Similarly, Fig. 1(d) shows the transition region of Boat image for Parida et al. [18] and the enlarged region R is displayed in Fig. 1(g). From Fig. 1(g) it is evident that the transition region also suffers from discontinuity issue as that of [15] which is well marked in blue lines. So, the segmentation mask obtained is distorted (missing some foreground region) affecting the overall segmentation result and performance. But the proposed method attains a better transition region compared to the former which can be visualized in Fig. 1(c) and enlarged version of R in Fig. 1(f). Therefore, it results in better segmentation mask as in Fig. 2(c) and better segmented object as in Fig. 2(f). So far the transition region based techniques developed do not perform well when the background is textured. The decomposition process can be visualized from Fig. 3.

In the proposed method, the image is decomposed in wavelet domain with four bands LL, LH, HL and HH [24]. The Boat image considered is having both foreground and background to be textured. The foreground is more textured compared to the background. In the LL band of wavelet domain, the foreground coefficients are more prominent suppressing the background texture. So, the extraction of coefficient corresponding to transition region between background and foreground becomes easier. The local standard deviation filtering followed by thresholding is applied independently on LL band to find the prominent coefficients. Using these prominent approximate coefficients of LL band, the corresponding coefficients for other bands are retained. Inverse wavelet transform is applied on the modified coefficients to get feature image. On the feature image Otsu thresholding applies to extract transition region. Morphological thinning applies to get continuous contours. Morphological region filling operation is applied on these contours to get object regions. Finally, the objects are separated from the object regions.

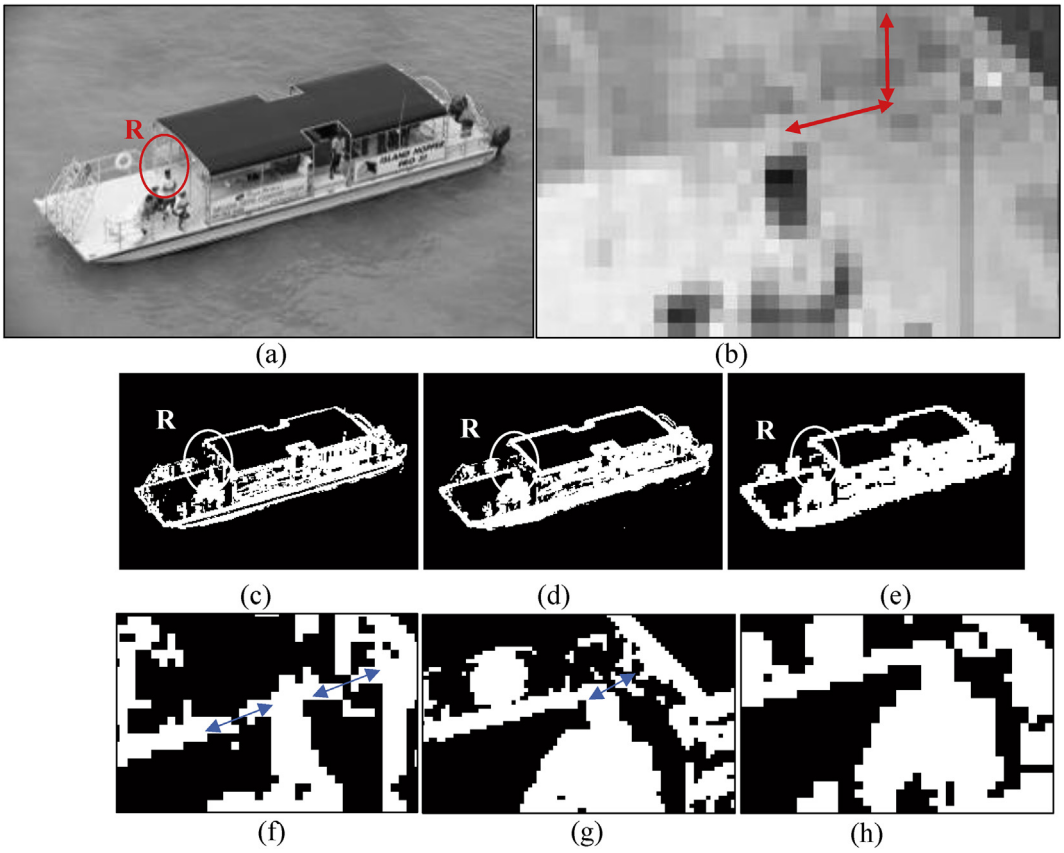

Fig. 1. Transition region extraction of Boat image: (a) Original gray image, (b) Zoomed region R of gray image, (c) Parida et al. [15], (d) Parida et al. [18], (e) Proposed method transition region, (f) Zoomed region R, (g) Zoomed region R, (h) Zoomed region R.

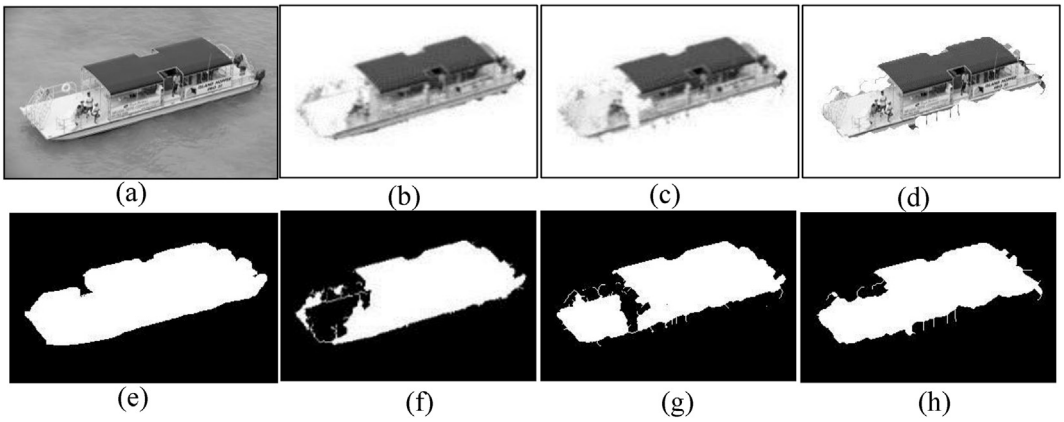

Fig. 2. Segmentation result and segmentation mask of Boat image for various methods: (a) Gray image, (b) Segmentation result of Parida et al. [15], (c) Segmentation result of Parida et al. [18], (d) Segmentation result of proposed method, (e) Ground truth, (f) Segmentation mask of Parida et al. [15], (g) Segmentation mask of Parida et al. [18], (h) Segmentation mask of proposed method.

The rest of the paper is organized as follows: Section 4 discusses the proposed method elaborately. Various quantitative measures for detecting the quality of the segmentation are provided in Section 5. The choice of wavelet basis function is discussed in Section 6. Section 7 discusses the comparison of proposed method with other method results. Section 6 provides the application of the proposed method to colour images in separating worms from leaves. Finally, the paper is concluded in Section 8.

4. Proposed method

The proposed method starts with decomposition of the original gray image in wavelet domain. In LL band the foreground is more prominent suppressing the background textures. This leads to an easier extraction of the transition region between foreground and background. The local standard deviation filtering and thresholding are applied on LL band for identifying the prominent features. Further, using the above-

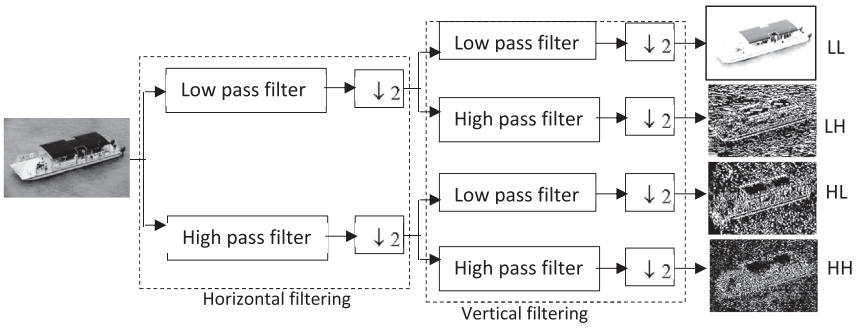

Fig. 3. Decomposition of Boat image using two dimensional discrete wavelet transform.

mentioned technique the detailed prominent coefficients are kept. Inverse wavelet transform is applied on the modified approximate coefficients and detailed coefficients to get an edge image with over one-pixel width. Further, Otsu thresholding is used on the edge image to extract transition regions. Morphological thinning and region filling operation is used on the transition region to extract the object regions. Finally, objects are extracted via these object regions. Fig. 4 shows the architecture of the proposed method.

4.1. Wavelet decomposition of image

Wavelets transform is an effective tool for time-frequency analysis. Various wavelet family exist in literature [25,26]. The input image is subjected to a two dimensional discrete wavelet transform. The image is decomposed into approximate, horizontal, vertical and detailed coefficient matrices. The approximate coefficients represent low frequency components whereas the detailed coefficients (horizontal, vertical and diagonal) represent the high frequency components which provides both high frequency values for both background and foreground (i.e. both edge and none edge regions). This can be better visualized from Fig. 3.

4.2. Extraction of high frequency information of object regions

In decomposition process from the former step, the high and low frequency components and the background and the foreground texture information are discriminated. The next goal is to retain prominent coefficients corresponding to the object regions. So, to extract these coefficients near the object boundary, the LL band is subjected to the object boundary extraction using local standard deviation filtering followed by global

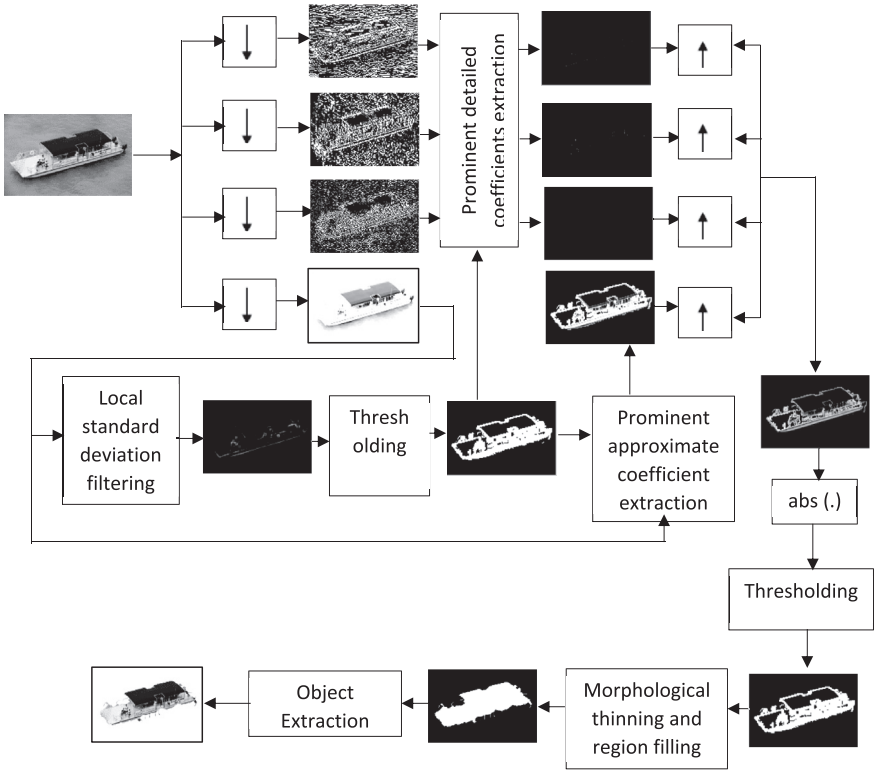

Fig. 4. Architecture of the proposed method for image segmentation.

thresholding. The local standard deviation of the approximate coefficients denoted by LS enhances the boundary regions sharply. The local standard deviation for a $m \times m$ neighbourhood centred at pixel $p(i,j)$ is calculated as

$$LS(i,j) = \sqrt{\frac{1}{m^2-1}\sum_{x=1}^{m}\sum_{y=1}^{m}\left(f(x,y)-\overline{f}\right)^2}, \quad \begin{matrix} i = 1,2,.....M \\ j = 1,2,.....N \end{matrix} \tag{1}$$

where the (x,y) denote a local coordinate in a given neighbourhood of the sub image f and $\overline{f}$ is the gray level mean of that neighbourhood. The M and N are the width and height of the image, respectively.

The above process is applied throughout the image by sliding the window from left to right and top to bottom to achieve the following standard deviation feature matrix

$$LS = \begin{bmatrix} LS(1,1) & LS(1,2) & ... & LS(1,N) \\ LS(2,1) & LS(2,2) & ... & LS(2,N) \\ ... & ... & ... & ... \\ LS(M,1) & LS(M,2) & ... & LS(M,N) \end{bmatrix} \tag{2}$$

where, M and N are the height and width of the image.

To extract the boundary regions, the feature image is further subjected to a global thresholding process where the mean of the feature image is chosen as the threshold. The thresholding is done as

$$F_T(i,j) = \begin{cases} 1 & if\ LS(i,j) \geq T; \\ 0 & otherwise, \end{cases} \tag{3}$$

where, F_T is the thresholded feature image and T is the global threshold calculated as

$$T = \frac{1}{M \times N}\sum_{k=1}^{M}\sum_{l=1}^{N} LS(k,l) \tag{4}$$

where, LS is the feature image of height M and width N. $LS(k,l)$ is the coefficient of the feature matrix at coordinate (k,l).

The thresholded feature matrix consists of 1 and 0 where 1 represent the pixel surrounding the object. Using the 1 values the new approximate and detail (horizontal, vertical and diagonal) coefficient matrices are extracted. The new detail coefficients represent only high frequency components of the boundary regions surrounding the objects.

4.3. Reconstruction of wavelet feature image and extraction of transition region

The wavelet feature image is reconstructed from the new detailed coefficients as well as the new approximate matrix obtained from the former step using inverse discrete wavelet transform. For the reconstruction of feature image, we have used Haar wavelet with a single level decomposition. The reason of using Haar wavelet is discussed in Section 6. On this

Table 1
Performance measures of Signboard and Boat images for different wavelet basis functions and levels.

Sl.No.	Image	Wavelet	Number of tap	ME	FPR	FNR	JI	SA
1	Signboard	Daubachies	1	0.0374	0.0476	0.0000	0.8517	0.9626
		Daubachies	2	0.0384	0.0412	0.0000	0.8688	0.9298
		Daubachies	3	0.0435	0.0554	0.0000	0.8314	0.9565
		Daubachies	4	0.0580	0.0737	0.0006	0.7871	0.9420
		Haar	1	0.0374	0.0476	0.0000	0.8517	0.9626
		Bi-orthogonal	1.1	0.0374	0.0476	0.0000	0.8517	0.9626
		Bi-orthogonal	1.3	0.0441	0.0562	0.0000	0.8294	0.9559
		Bi-orthogonal	1.5	0.0455	0.0579	0.0000	0.8250	0.9545
		Bi-orthogonal	2.2	0.0374	0.0476	0.0000	0.8517	0.9626
		Bi-orthogonal	2.4	0.0465	0.0592	0.0000	0.8219	0.9535
		Coiflets	1	0.0344	0.0438	0.0000	0.8618	0.9656
		Coiflets	2	0.0466	0.0591	0.0008	0.8215	0.9534
		Symlets	1	0.0374	0.0476	0.0000	0.8517	0.9626
		Symlets	2	0.0324	0.0412	0.0000	0.8688	0.9676
		Symlets	3	0.0435	0.0554	0.0000	0.8314	0.9565
2	Boat	Daubachies	1	0.0536	0.0027	0.1724	0.8225	0.9464
		Daubachies	2	0.0735	0.0007	0.2431	0.7558	0.9265
		Daubachies	3	0.0974	0.0025	0.3186	0.6775	0.9026
		Daubachies	4	0.0923	0.0173	0.2670	0.7046	0.9077
		Haar	1	0.0536	0.0027	0.1724	0.8225	0.9464
		Bi-orthogonal	1.1	0.0536	0.0027	0.1724	0.8225	0.9464
		Bi-orthogonal	1.3	0.0540	0.0065	0.1645	0.8230	0.9460
		Bi-orthogonal	1.5	0.0553	0.0075	0.1666	0.8190	0.9447
		Bi-orthogonal	2.2	0.0656	0.0029	0.2118	0.7829	0.9344
		Bi-orthogonal	2.4	0.0659	0.0058	0.2061	0.7834	0.9341
		Coiflets	1	0.0990	0.0003	0.3289	0.6707	0.9010
		Coiflets	2	0.1027	0.0035	0.3336	0.6609	0.8973
		Symlets	1	0.0536	0.0027	0.1724	0.8225	0.9464
		Symlets	2	0.0735	0.0007	0.2431	0.7558	0.9265
		Symlets	3	0.0974	0.0025	0.3186	0.6775	0.9026

feature image we apply Otsu thresholding to get transition region.

4.4. Morphological thinning and region filling operation

The transition regions having more than one-pixel width are generated from the former step. These transition regions undergo morphological thinning operation to yield object contours of a single pixel width. The object contours obtained are all continuous. We apply morphological region filling operation which results in the extraction of object regions from the object contours. The structuring element used for morphological thinning and region filling operation is of disk type with radius 3.

4.5. Object extraction

The object region extracted from the previous step is a binary image where the object regions are marked with value 1 and background as 0. This also referred as segmentation mask. From the segmentation mask the segmented object is extracted by replacing the 1 with the original gray value from the input image and the background 0 is replaced by a value 255.

5. Performance measures

The performance of the proposed method is quantitatively evaluated via 5 different performance measures: misclassification error (ME) [27,28], false positive rate (FPR) [28], false negative rate (FNR) [28], Jaccard index (JI) [29] and segmentation accuracy (SA) [30].

In a binary classification, the foreground (object) pixels erroneously classified as background or vice versa is termed as misclassification error (ME) [27]. The ME is defined as

$$ME = 1 - \frac{|B_O \cap B_T| + |F_O \cap F_T|}{|B_O| + |F_O|} \tag{5}$$

where the B_O and F_O denote the background and object pixels of ground truth image whereas B_T and F_T represent the background and foreground pixels of the segmentation result. The operator $|.|$ represent the cardinality of a set operation. The ME value lie between 0 and 1 where 0 represent complete segmentation without any deviation from ground truth. The value 1 correspond to totally erroneous segmentation result. The less the value of ME correspond to better segmentation result. The measures FPR and FNR define the former measure more precisely.

The FPR is the number of background pixels classified as object pixels to the total number of background pixel. The FNR is the number of pixels in the object classified in the background pixels to total object pixels. The FPR and FNR is defined as

$$FPR = \frac{|B_O \cap F_T|}{|B_O|} \tag{6}$$

$$FNR = \frac{|F_O \cap B_T|}{|F_O|} \tag{7}$$

The value of FPR and FNR also varies between 0 and 1. The lower the value of FPR and FNR, the better is segmentation result. Higher values of FPR and FNR makes the result to be highly over segmentation and under segmentation, respectively.

To evaluate the similarity of the segmentation result with the ground truth, Jaccard index is used. The Jaccard index [29] is defined as

$$JI = \frac{|GT \cap SR|}{|GT \cup SR|} \tag{8}$$

where the, GT and SR correspond to ground truth and segmentation result, respectively. The JI value varies between 0 and 1. Higher value (i.e., close to 1) denote better segmentation result or maximum resemblance with the ground truth (required segmentation result).

Segmentation accuracy (SA) [30] is a global measure which denote the ratio of total well classified pixels in the segmentation result which is given as

$$SA = \frac{Number\ of\ correctly\ segmented\ pixels}{Total\ number\ of\ pixels} \tag{9}$$

The value of SA remains in the range from 0 to 1. High SA value indicate better segmentation accuracy. Based on the above five performance measures the proposed method is quantitatively compared with various segmentation methods.

6. Choice of wavelet basis function

The choice of a proper wavelet basis function depends upon various applications such as enhancement, de-noising, texture feature extraction, etc. The proposed method is tested by applying Haar, Daubechies, Coiflets, Symlet and Bi-orthogonal wavelet families with different decomposition levels are tested against the all performance measures (ME, FPR, FNR, JI and SA) for different images. For a single level decomposition and 1-tap the Haar, Daubechies, Coiflets and Symlet basis functions outperforms well. This can be well verified from Table 1 where we have determined the various performance measures of the proposed method for Signboard and Boat image. For both Signboard and Boat image the proposed method achieves good ME, FPR, FNR using a single level decomposition and 1-tap filter for Haar, Daubechies, Coiflets and Symlet wavelet family. As the Haar basis function is simple and can be easily implemented in hardware, we have used Haar wavelet as our basis function for both decomposition and reconstruction.

7. Result and discussion

The entire experiment is performed in a PC with Core-i3, 1.9 GHz processor and 8 GB RAM. The experimentation is done in MATLAB 7.0 environment. The proposed method is

Table 2
Performance measures (ME, FPR, FNR, JI, SA) of different methods for various types of images.

Sl.no.	Image	Methods	ME	FPR	FNR	JI	SA
1	Aeroplane	LE	0.0630	0.0666	**0.0031**	0.4752	0.9370
		MLE	0.0263	0.0248	0.0507	0.6726	0.9737
		LGLD	0.9637	1.0000	0.5466	0.0363	0.0019
		RIB	**0.0097**	**0.0087**	0.0263	**0.8510**	**0.9903**
		Parida et al. [15]	0.0179	0.0089	0.1670	0.7269	0.9821
		Parida et al. [18]	0.0211	0.0089	0.2224	0.6781	0.9789
		Proposed method	0.0217	0.0088	0.2348	0.6688	0.9783
2	Eagle	LE	0.2992	0.3165	**0.0000**	0.1546	0.7008
		MLE	0.0534	0.0308	0.4460	0.3607	0.9466
		LGLD	0.8009	0.7915	0.9633	0.0025	0.1991
		RIB	0.0159	0.0167	0.0017	0.7742	0.9841
		Parida et al. [15]	**0.0065**	0.0047	0.0378	**0.8896**	**0.9935**
		Parida et al. [18]	0.0102	0.0049	0.1013	0.8286	0.9898
		Proposed method	0.0088	**0.0033**	0.1039	0.8472	0.9912
3	Bird	LE	0.0939	0.0990	**0.0072**	0.3696	0.9061
		MLE	0.0654	0.0414	0.4808	0.3028	0.9346
		LGLD	0.9792	0.9901	0.7932	0.0116	0.0208
		RIB	0.0369	0.0202	0.3245	0.5006	0.9631
		Parida et al. [15]	0.0274	0.0192	0.1684	0.6269	0.9726
		Parida et al. [18]	0.0256	0.0148	0.2084	0.6320	0.9744
		Proposed method	**0.0224**	**0.0109**	0.2181	**0.6593**	**0.9776**
4	Boat	LE	0.2435	0.2658	0.1916	0.4993	0.7565
		MLE	0.1871	0.0436	0.5243	0.4316	0.8129
		LGLD	0.7307	0.8330	0.4924	0.1726	0.2693
		RIB	0.1784	0.0121	0.5688	0.4193	0.8216
		Parida et al. [15]	0.0622	**0.0017**	0.2032	0.7936	0.9378
		Parida et al. [18]	0.0578	0.0021	0.1875	0.8086	0.9422
		Proposed method	**0.0536**	0.0027	**0.1724**	**0.8225**	**0.9464**
5	Signboard-1	LE	0.8661	0.9544	0.5426	0.1017	0.1339
		MLE	0.8047	0.8062	0.7995	0.0506	0.1953
		LGLD	0.0889	0.0525	0.2222	0.6524	0.9111
		RIB	0.0709	0.0901	0.0000	0.7513	0.9291
		Parida et al. [15]	0.3899	0.4964	0.0000	0.3549	0.6101
		Parida et al. [18]	0.0497	0.0632	0.0000	0.8119	0.9503
		Proposed method	**0.0374**	**0.0476**	**0.0000**	**0.8517**	**0.9626**
6	Flower-1	LE	0.5883	0.7238	0.2192	0.2627	0.4117
		MLE	0.3441	0.1458	0.8871	0.0807	0.6559
		LGLD	**0.0114**	**0.0005**	0.0410	0.9577	**0.9886**
		RIB	0.0149	0.0202	**0.0006**	0.9471	0.9851
		Parida et al. [15]	0.0184	0.0186	0.0177	0.9349	0.9816
		Parida et al. [18]	0.0167	0.0165	0.0171	0.9406	0.9833
		Proposed method	0.0115	0.0088	0.0186	**0.9583**	0.9787
7	Papaya	LE	0.5925	0.7658	0.3835	0.3205	0.4075
		MLE	0.3266	0.0638	0.6455	0.3291	0.6734
		LGLD	0.1277	0.0000	0.2816	0.7184	0.8723
		RIB	0.3204	**0.0000**	0.7093	0.2907	0.6796
		Parida et al. [15]	0.0199	0.0153	**0.0254**	0.9570	0.9801
		Parida et al. [18]	0.0195	0.0122	0.0284	0.9576	0.9805
		Proposed method	**0.0133**	0.0010	0.0281	**0.9708**	**0.9867**
8	Players	LE	0.3179	0.3310	0.1492	0.1612	0.6821
		MLE	0.1710	0.1439	0.5243	0.1656	0.8290
		LGLD	0.8065	0.8585	0.1342	0.0716	0.1935
		RIB	0.1557	0.0909	1.0000	0.0000	0.8443
		Parida et al. [15]	0.0824	0.0807	**0.1048**	0.4382	0.9176
		Parida et al. [18]	0.0979	0.0950	0.1357	0.3880	0.9021
		Proposed method	**0.0744**	**0.0679**	0.1579	**0.4485**	**0.9256**
9	Player	LE	0.1752	0.2011	**0.0751**	0.5205	0.8248
		MLE	0.1814	0.0455	0.7093	0.2470	0.8186
		LGLD	0.1250	0.0747	0.3194	0.5283	0.8750
		RIB	0.1911	0.0144	0.8778	0.1157	0.8089
		Parida et al. [15]	0.0405	**0.0120**	0.1509	0.8116	0.9595
		Parida et al. [18]	0.0405	0.0215	0.1142	0.8179	0.9595
		Proposed method	**0.0363**	0.0159	0.1153	**0.8336**	**0.9637**

Table 2 (*continued*)

Sl.no.	Image	Methods	ME	FPR	FNR	JI	SA
10	Puppy	LE	0.3686	0.4111	0.2777	0.3846	0.6314
		MLE	0.3379	0.0787	0.8941	0.0906	0.6621
		LGLD	**0.0191**	**0.0030**	0.0537	**0.9404**	**0.9809**
		RIB	0.3169	0.0070	0.9821	0.0177	0.6831
		Parida et al. [15]	0.3074	0.0201	0.9211	0.0756	0.6926
		Parida et al. [18]	0.0354	0.0443	**0.0162**	0.8987	0.9646
		Proposed method	0.0245	0.0251	0.0233	0.9269	0.9755

The best values of each performance measures for each image are marked in bold.

compared with several existing transition region based methods such as LE [19], MLE [14], LGLD [17], RIB [13], Parida et al. [15] and Parida et al. [18]. The images used for experimentation are 8-bit and of different resolution to demonstrate the effectiveness of proposed method under various resolutions. The images contain both single and multiple objects in the experimentation process.

To begin our analysis, the images along with their corresponding ground truths considered for experimentation are taken from Wisemann dataset [23] and MSRM database [31]. The images contain both single and multiple images with both foreground/background simple and textured. For each image we have computed five quantitative measures such as ME, FPR, FNR, JI and SA for various methods along with our proposed method which are listed in Table 2. The qualitative evaluation can be verified from the segmentation masks and the segmentation results shown in Fig. 6 and Fig. 5 respectively.

We have considered images of simple as well as textured background/foreground in our experimentation to show the effectiveness of our method. The Aeroplane image is a single object image with simple foreground and background. From Table 2, the best ME, FPR, JI and SA values for Aeroplane image is provided by the method RIB. The method LE attains the lowest FNR indicating that the result is not under-segmented. But, visual perception indicates that LE retains more background portions as compared to others. Fig. 5 indicates that almost all methods segment the Aeroplane image effectively. The proposed method attains a less performance value than RIB, but Table 2 indicate that the results of the proposed method is very close to that of RIB. For Eagle image the foreground is simple but the background is a bit textured with varying intensities. The method Parida et al. [15] attains the best ME, JI and SA values, whereas the proposed method and RIB provide the lowest FPR and FNR respectively. From Table 2 it can be verified that the proposed method attains an approximately equal value of performance as that of Parida et al. [15]. The segmentation results correlate the above-mentioned facts in Fig. 5. The Bird image is a multi-object image with simple foreground and background. For Bird image, the proposed method attains the best values of ME, FPR, JI and SA. This indicate that the proposed method extracts multiple objects effectively and the result is not over-segmented as compared to others. The best FNR value for Bird image is given by the method LE but it retains most foreground regions which can be verified from Fig. 5. The Boat image is a complex image with textured foreground and background. For Boat image, the proposed method attains lowest value of ME, FNR and highest JI, SA respectively. This can be visually verified from the segmentation masks of the Boat image provided in Fig. 6. The performance of the other transition region based approaches degrades due to the ineffective transition region extraction as discussed in the earlier section of the paper. The results obtained by the existing approaches either loses some object regions or emerges some background regions in the segmentation result. But the proposed approach effectively segments the object with less emergence of background regions and low loss of object regions. The Signboard image is a single object image with textured background and simple foreground. The method LSISIM achieves the best values of ME, FPR, JI and SA. The lowest FNR is provided by the proposed method. But comparison of the segmentation mask in Fig. 6 indicate that the proposed method achieves the approximate result as that of LSISIM. The proposed method as it supress the background texture achieve better segmentation output as compared to existing approaches. For Flower image, the method LGLD attains the lowest ME, FPR with highest SA. The method RIB attains lowest FNR indicating that the result is not under-segmented. The proposed method attains highest JI indicating the maximum similarity with the ground truth. The proposed approach attains nearly equal performance measures as that of LGLD which can be verified from Table 2. For Papaya image, which consists of textured foreground with simple background, the proposed method attains the best values of ME, JI and SA. The best FPR is provided by RIB indicating the result is not over-segmented. But, due to inaccurate transition region extraction the method RIB loses majority foreground regions which is not desirable. Similarly, for Players image comprising of multiple images the proposed method attains the best ME, FPR, JI and SA values. The method LGLD attains the lowest FNR for Players image. The performance of the proposed approach is better in comparison to other approaches is due to the suppression of background texture and extracting an effective transition region as compared to existing transition region approaches. Similarly, for Player image, the proposed method outperforms well in all aspects except for the FPR and FNR. The method LE has the best

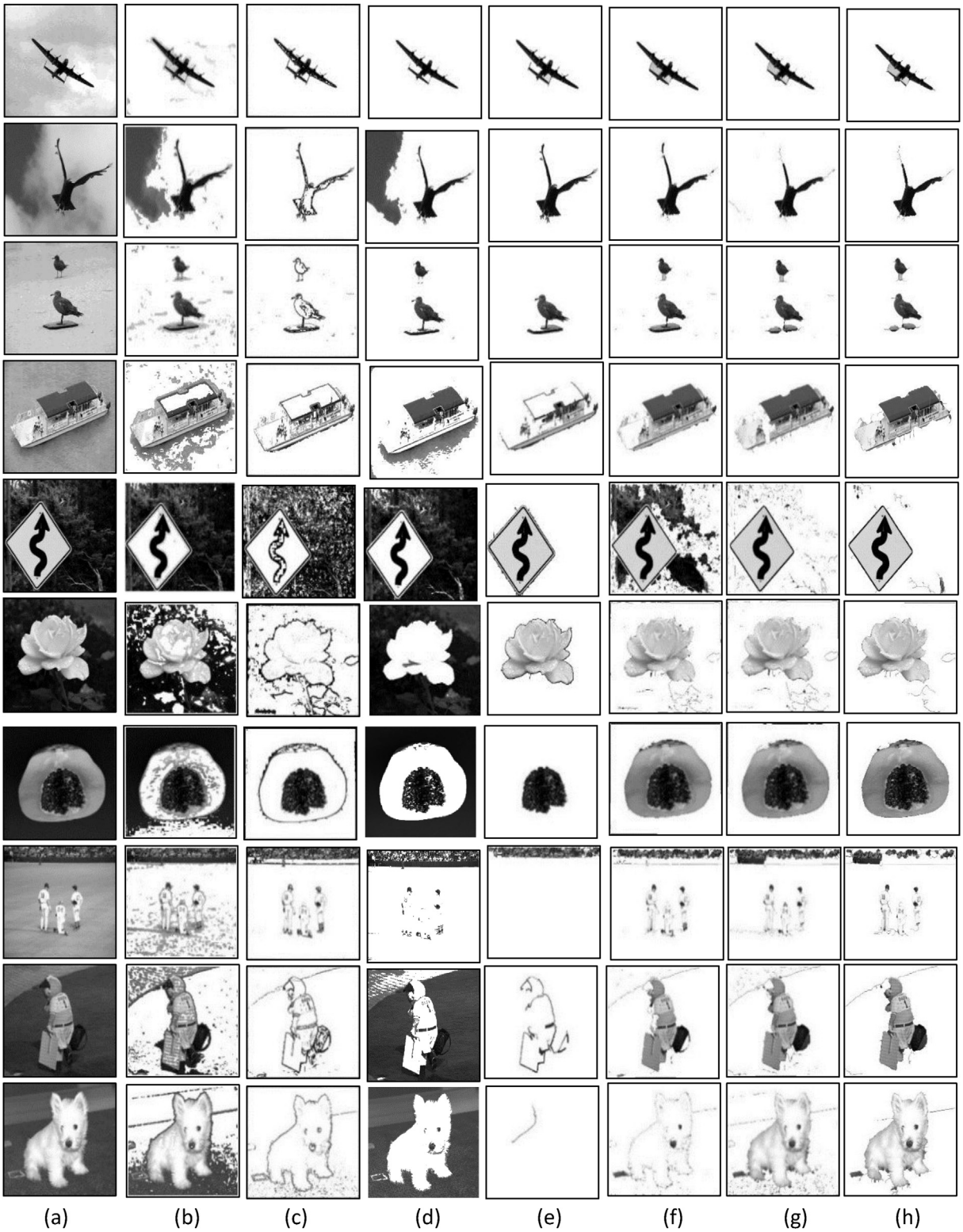

Fig. 5. Segmentation result of various methods for different images: Aeroplane, Eagle, Bird, Boat, Signboard, Flower, Papaya, Players, Player and Puppy. (a) Original gray image, (b) LE, (c) MLE, (d) LGLD, (e) RIB, (f) Parida et al. [15], (g) Parida et al. [18], (h) Proposed method.

FNR but visual inspection from Fig. 6 reveal that the proposed method provides better segmentation result in comparison to existing methods. The Puppy image has the foreground and background region has sharp varying intensities. The foreground also contains some texture portion. Despite of these conditions, the proposed method achieves better ME. The method LGLD attains lowest FPR, JI, SA and [18] attains lowest FNR. This indicates that the

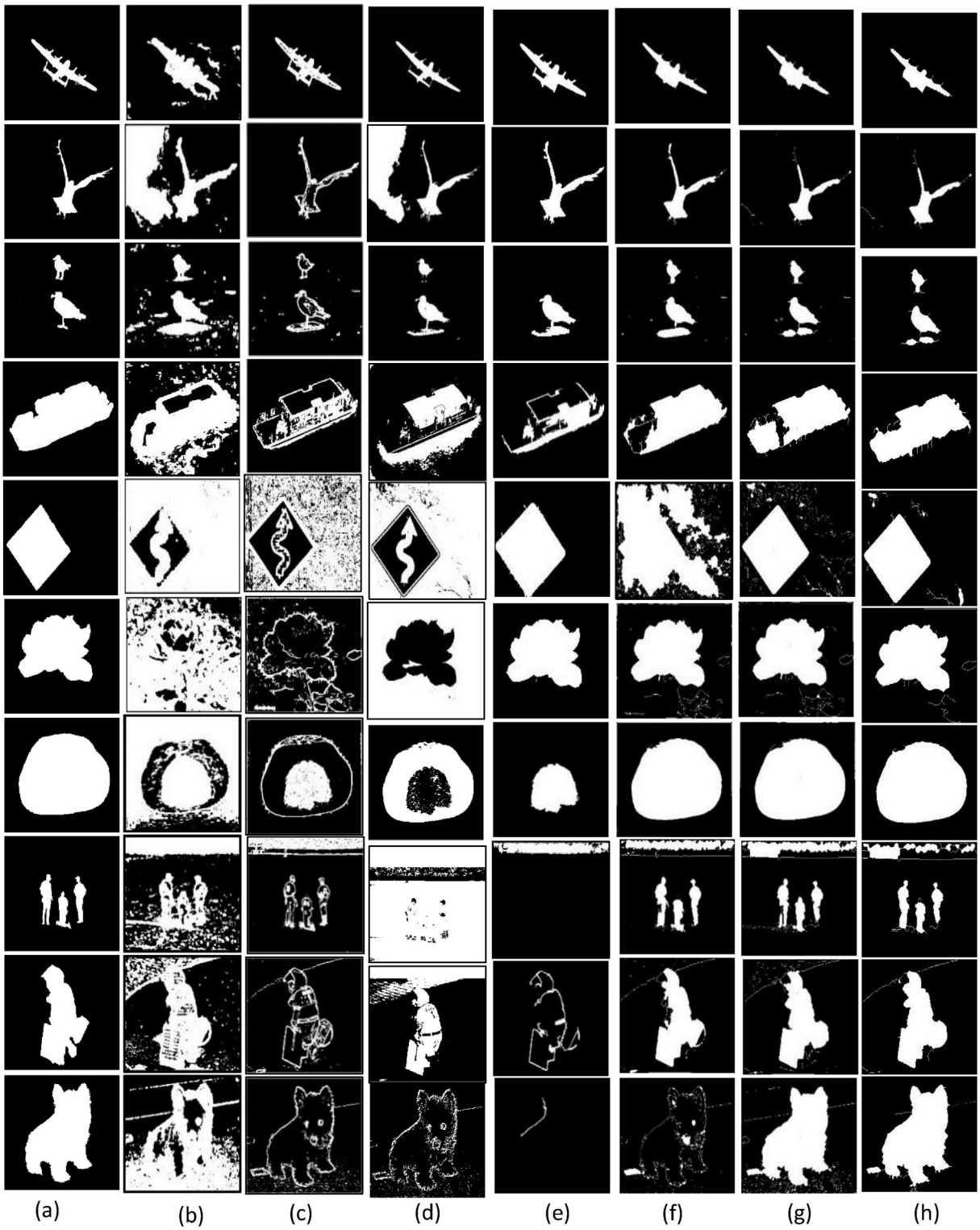

Fig. 6. Segmentation masks of various methods for different images: Aeroplane, Eagle, Bird, Boat, Signboard, Flower, Papaya, Players, Player and Puppy. (a) Ground truth, (b) LE, (c) MLE, (d) LGLD, (e) RIB, (f) Parida et al. [15], (g) Parida et al. [18], (h) Proposed method.

proposed method also provides better segmentation result in case of textured foreground. It can be clarified visually from the segmentation masks in Fig. 6.

To show the effectiveness of the proposed method in comparison with other methods their average performance measure is calculated for all images and are given in Table 3. From Table 3 it is evident that the proposed method has the lowest average ME, FPR and FNR. Hence, the proposed method can be treated as the better method as compared to others.

Table 3
Average performance of different methods for various performance measures.

Method	Average ME	Average FPR	Average FNR
LE	0.3608	0.4135	0.1849
MLE	0.2498	0.1425	0.5962
LGLD	0.4653	0.4604	0.3848
RIB	0.1311	0.0280	0.4491
Parida et al. [15]	0.0973	0.0678	0.1796
Parida et al. [18]	0.0374	0.0283	0.1031
Proposed method	**0.0282**	**0.0183**	**0.0838**

The best average values of different performance measures are marked in bold.

8. Application of the proposed method in worm separation from leaves

The proposed method is applied for worm separation from leaf using the colour image as input. The detailed architecture is given in Fig. 7.

Initially the original RGB image is converted to CIE-Lab colour space which enhances the image. Further, the components are separated and the L-component that closely matches the human perception of lightness is used for

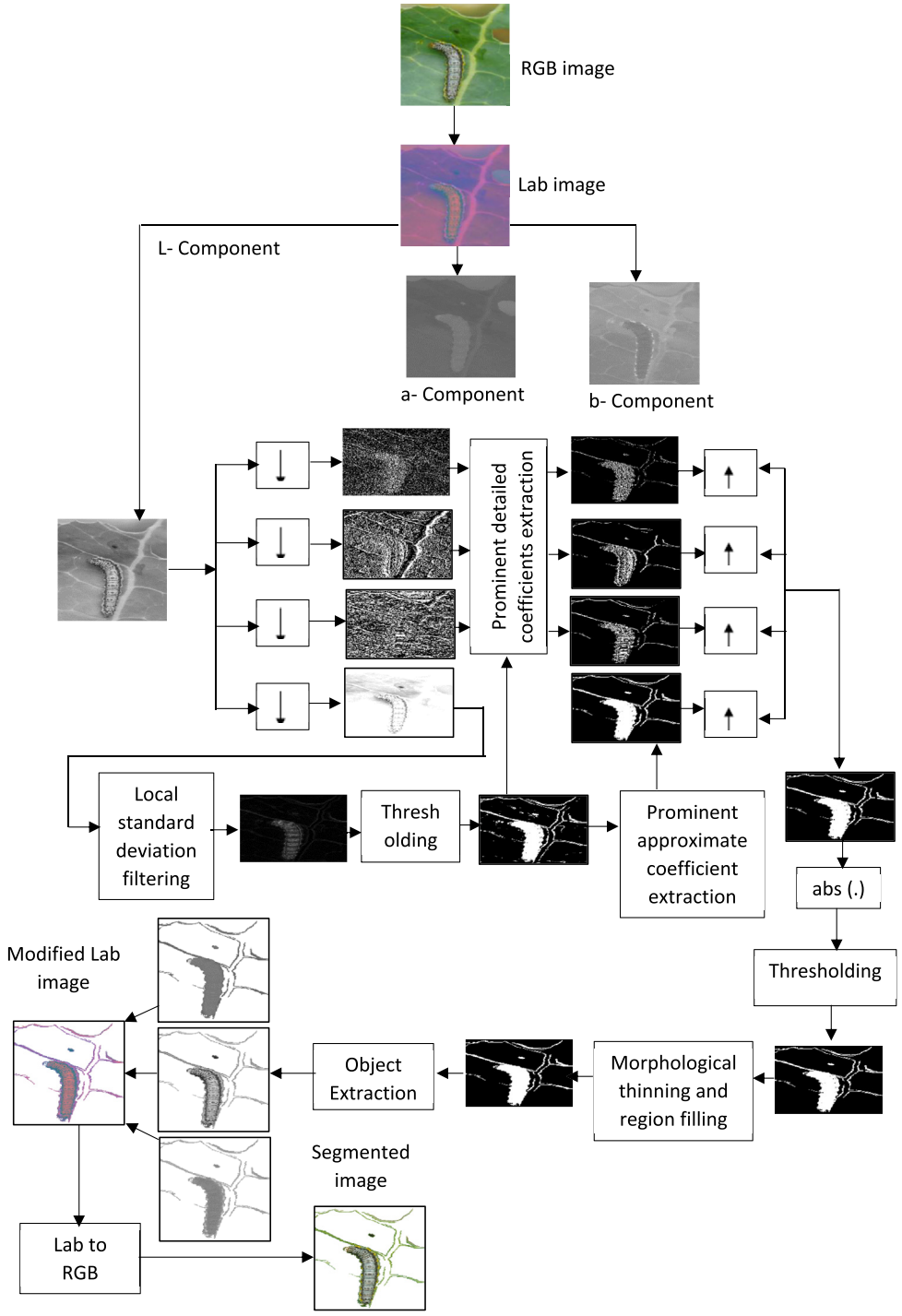

Fig. 7. Architecture of the proposed method for worm separation from leaf.

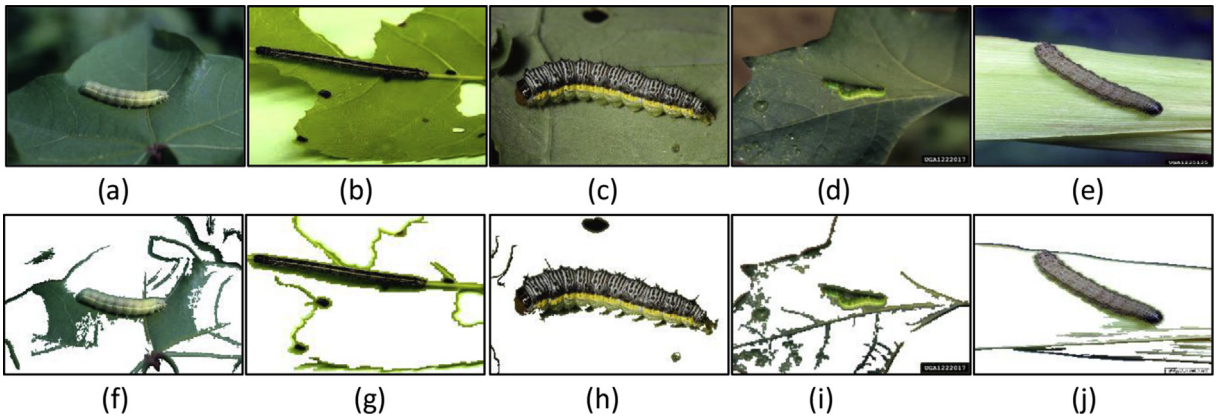

Fig. 8. Different types of worms in different leaves and their segmentation result using proposed approach: (a) Beet army worm, (b) Cankerworm, (c) Cross stripped cabbage worm, (d) Cotton leaf worm, (e) Fall army worm, (f) Segmentation result of (a), (g) Segmentation result of (b), (h) Segmentation result of (c), (i) Segmentation result of (d), (j) Segmentation result of (e).

subsequent processing. The L-component is decomposed using 2-dimensional discrete wavelet transform of 1 level giving rise to LL, LH, HL and HH bands. Further, local standard deviation filtering along with thresholding is applied on LL band to identify the prominent coefficients. From the prominent coefficients, the modified LL, LH, HL and HH coefficients are extracted which is used to reconstruct the feature matrix using inverse discrete wavelet transform. The transition regions are extracted by applying Otsu thresholding [32]. The transition regions extracted are further filled using morphological region filling to find the object regions. The R, G and B components of the original RGB image are replaced with regions having value 1 in object region image to find the segmented object.

To show the effectiveness of the aforementioned method we have collected several worm images from the Bugwood image dataset [33] for different types of leaves. The segmentation results along with the original image are given in Fig. 8. It can be visualized from Fig. 8 that for almost all sorts of worms can be separated from leaf image using the proposed approach. Although, some background portions appear in the segmented result, the worms are accurately separated.

9. Conclusion

The paper presents a new transition extraction method using wavelet transformed local features for image segmentation. The transition region extracted is robust in the sense that the proposed method is able to extract the exact transition region correctly for all types of images (i.e. for both foreground and background simple as well as textured). The method suppress background texture features enhancing foreground features for achieving better segmentation. Experimental results indicate that the proposed method achieves better results in low as well as high intensity varying conditions between foreground and background. The proposed method works well for both single and multiple objects and the results obtained has less emergence of background and low loss of object regions. The proposed method also works well for colour images. The method effectively works in separation of worms from leaf image which can be helpful for farmers for better yield of crops.

References

[1] Mondal S, Bours P. Neurocomputing A study on continuous authentication using a combination of keystroke and mouse biometrics. Neurocomputing 2017;230:1–22. https://doi.org/10.1016/j.neucom.2016.11.031.

[2] Iii WMW, Mondal S, Bours P, Akram T, Naqvi SR, Haider SA, et al. Medical Image Analysis – past , present , and future. Comput Electr Eng 2017;59:1–22. https://doi.org/10.1016/j.neucom.2016.11.031.

[3] Akram T, Naqvi SR, Haider SA, Kamran M. Towards real-time crops surveillance for disease classification : exploiting parallelism in computer vision R. Comput Electr Eng 2017;59:15–26. https://doi.org/10.1016/j.compeleceng.2017.02.020.

[4] Xia Y, Ji Z, Zhang Y. Brain MRI image segmentation based on learning local variational Gaussian mixture models. Neurocomputing 2016;204:189–97. https://doi.org/10.1016/j.neucom.2015.08.125.

[5] Ji Z, Xia Y, Sun Q, Chen Q, Feng D. Adaptive scale fuzzy local Gaussian mixture model for brain MR image segmentation. Neurocomputing 2014;134:60–9. https://doi.org/10.1016/j.neucom.2012.12.067.

[6] Ren Malik. Learning a classification model for segmentation. In: Proceedings Ninth IEEE International conference on computer vision, vol. 1. IEEE; 2003. p. 10–7. https://doi.org/10.1109/ICCV.2003.1238308.

[7] Boykov YY, Jolly M-P. Interactive graph cuts for optimal boundary & region segmentation of objects in N-D images. In: Proceedings Eighth IEEE International conference on computer vision. ICCV 2001, vol. 1, IEEE comput. Soc; 2001. p. 105–12. https://doi.org/10.1109/ICCV.2001.937505.

[8] Jin R, Yin J, Zhou W, Yang J. Level set segmentation algorithm for high-resolution polarimetric SAR images based on a heterogeneous clutter model. IEEE J Sel Top Appl Earth Obs Rem Sens 2017:1–15. https://doi.org/10.1109/JSTARS.2017.2716620.

[9] Zhou Y, Shi W-R, Chen W, Chen Y, Li Y, Tan L-W, et al. Active contours driven by localizing region and edge-based intensity fitting energy with application to segmentation of the left ventricle in cardiac CT images. Neurocomputing 2015;156:199–210. https://doi.org/10.1016/j.neucom.2014.12.061.

[10] Kass M, Witkin A, Terzopoulos D. Snakes: active contour models. Int J Comput Vis 1988;1:321–31. https://doi.org/10.1007/BF00133570.

[11] Chen Y, Zhang J, Mishra A, Yang J. Image segmentation and bias correction via an improved level set method. Neurocomputing 2011;74:3520–30. https://doi.org/10.1016/j.neucom.2011.06.006.

[12] Zhang YJJ, Gerbrands JJJ. Transition region determination based thresholding. Pattern Recogn Lett 1991;12:13−23. https://doi.org/10.1016/0167-8655(91)90023-F.

[13] Li Z, Liu G, Zhang D, Xu Y. Robust single-object image segmentation based on salient transition region. Pattern Recogn 2016;52:317−31. https://doi.org/10.1016/j.patcog.2015.10.009.

[14] Li Z, Zhang D, Xu Y, Liu C. Modified local entropy-based transition region extraction and thresholding. Appl Soft Comput J 2011;11:5630−8. https://doi.org/10.1016/j.asoc.2011.04.001.

[15] Parida P, Bhoi N. Transition region based single and multiple object segmentation of gray scale images. Eng Sci Technol Int J 2016;19:1206−15. https://doi.org/10.1016/j.jestch.2015.12.009.

[16] Behera SK, Parida P, Bhoi N, Athghara AK. An analytical review on various image segmentation methods based on transition region-based thresholding. Int J Adv Res Electr Electron Instrum Eng 2016;5:3845−52. https://doi.org/10.15662/IJAREEIE.2016.0505056.

[17] Li Z, Liu C. Gray level difference-based transition region extraction and thresholding. Comput Electr Eng 2009;35:696−704. https://doi.org/10.1016/j.compeleceng.2009.02.001.

[18] Parida P, Bhoi N. 2-D Gabor filter based transition region extraction and morphological operation for image segmentation. Comput Electr Eng 2017;62:119−34. https://doi.org/10.1016/j.compeleceng.2016.10.019.

[19] Yan C, Sang N, Zhang T. Local entropy-based transition region extraction and thresholding. Pattern Recogn Lett 2003;24:2935−41. https://doi.org/10.1016/S0167-8655(03)00154-5.

[20] Parida P, Bhoi N, Dewangan P. Colour image segmentation based on transition region and morphological operation. In: 2017 International conference on wireless communications, signal processing and networking (WiSPNET), vol. 62. IEEE; 2017. p. 1293−7. https://doi.org/10.1109/WiSPNET.2017.8299972.

[21] Parida P, Bhoi N. Wavelet based transition region extraction for image segmentation. Future Comput Inf J 2017;2:68−78. https://doi.org/10.1016/j.fcij.2017.10.005.

[22] Kim SC, Kang TJ. Texture classification and segmentation using wavelet packet frame and Gaussian mixture model. Pattern Recogn 2007;40:1207−21. https://doi.org/10.1016/j.patcog.2006.09.012.

[23] Alpert S, Galun M, Brandt A, Basri R. Image segmentation by probabilistic bottom-up aggregation and cue integration. IEEE Trans Pattern Anal Mach Intell 2012;34:315−27. https://doi.org/10.1109/TPAMI.2011.130.

[24] Guijarro M, Riomoros I, Pajares G, Zitinski P. Discrete wavelets transform for improving greenness image segmentation in agricultural images. Comput Electron Agric 2015;118:396−407. https://doi.org/10.1016/j.compag.2015.09.011.

[25] Bakhshipour A, Jafari A, Nassiri SM, Zare D. Weed segmentation using texture features extracted from wavelet sub-images. Biosyst Eng 2017;157:1−12. https://doi.org/10.1016/j.biosystemseng.2017.02.002.

[26] Khan MM, Mendes A, Zhang P, Chalup SK. Evolving multi-dimensional wavelet neural networks for classification using Cartesian Genetic Programming. Neurocomputing 2017;247:39−58. https://doi.org/10.1016/j.neucom.2017.03.048.

[27] Yasnoff WA, Mui JK, Bacus JW. Error measures for scene segmentation. Pattern Recogn 1977;9:217−31. https://doi.org/10.1016/0031-3203(77)90006-1.

[28] Sankur B. Survey over image thresholding techniques and quantitative performance evaluation. J Electron Imag 2004;13:146. https://doi.org/10.1117/1.1631315.

[29] Tizhoosh HR, Othman AA. Anatomy-aware measurement of segmentation accuracy. In: Styner MA, Angelini ED, editors. Proc. SPIE 9784, medical imaging 2016: image processing; 2016. p. 301−10. https://doi.org/10.1117/12.2214869.

[30] Rajaby E, Ahadi SM, Aghaeinia H. Robust color image segmentation using fuzzy c-means with weighted hue and intensity. Digit Signal Process 2016;51:170−83. https://doi.org/10.1016/j.dsp.2016.01.010.

[31] Liu T, Yuan Z, Sun J, Wang J, Zheng N, Tang X, et al. Learning to detect a salient object. IEEE Trans Pattern Anal Mach Intell 2011;33:353−67. https://doi.org/10.1109/TPAMI.2010.70.

[32] Otsu N. A threshold selection method from gray level histograms. IEEE Trans Syst Man Cybern 1979;9:62−6. https://doi.org/10.1109/TSMC.1979.4310076.

[33] Goëau H, Bonnet P, Joly A. The Image CLEF 2011 plant images classication task, vol. 2011; 2011.